CALPHAD: Computer Coupling of Phase Diagrams and Thermochemistry 46 (2014) 134–147

Contents lists available at ScienceDirect

CALPHAD: Computer Coupling of Phase Diagrams and Thermochemistry

journal homepage: www.elsevier.com/locate/calphad

# Critical assessment and thermodynamic modeling of Mg–Ca–Zn system supported by key experiments

M. Mezbahul-Islam, Y.N. Zhang, C. Shekhar, M. Medraj *

*Department of Mechanical Engineering, Concordia University, 1455 De Maisonneuve Blvd. West, Montreal, QC, Canada H3G 1M8*

ARTICLE INFO

*Article history:*
Received 20 November 2013
Received in revised form
8 March 2014
Accepted 10 March 2014
Available online 28 March 2014

*Keywords:*
Mg-based alloys
Mg–Ca–Zn
Thermodynamic modeling
Differential scanning calorimetry
CALPHAD

ABSTRACT

A self-consistent thermodynamic description of the Mg–Ca–Zn ternary system has been obtained in this work. Four ternary intermetallic compounds (IM1, IM2, IM3 and IM4) and binary compounds with extended ternary solubility have been included in the modeling. Binary compounds, $CaZn_{11}$ and $CaZn_{13}$ in the Ca–Zn system have been re-modeled by compound energy formalism (CEF) to accommodate recently reported ternary solubility ranges. Also $Mg_2Ca$ in the Mg–Ca system has been re-optimized. Among the ternary intermetallic compounds, IM1 and IM3 having complex solubility ranges have also been modeled using compound energy formalism, whereas IM2 and IM4 have been considered as stoichiometric phases. Modified quasi-chemical model (MQM) has been used to model the liquid phase in the system. To investigate the behavior of the system and to verify the consistency of the thermodynamic model with experimental results, key samples with 4 at% and 6 at% Ca concentration were prepared and characterized with differential scanning calorimeter (DSC). Various vertical sections, liquidus projection and isothermal section at 608 K, in the Mg–Ca–Zn system have been calculated and found to be in good agreement with the experimental data.



## 1. Introduction

With the increased demand of hydrocarbon based fuel and gradual increase in its price, the focus is shifting towards the fuel efficient transportation technologies [1,2]. Among different strategies, first approach to enhance the fuel efficiency is the reduction of vehicle body weight. Magnesium (Mg), being the lightest structural material, has attracted much attention to replace the heavier parts in the automotive and aerospace applications [1,2]. In order to achieve desired mechanical properties, Mg is alloyed with various elements. The addition of Ca to magnesium improves strength, castability, creep resistance, corrosion resistance [3] and oxidation resistance [4]. In addition, Zn has been found to increase the peak-hardness value and enhance the age hardening kinetics of the Mg–Ca alloys due to the formation of ternary precipitates [5] that have lower lattice mismatch with the Mg solid solution matrix [6,7]. Recently, Mg-rich Mg–Ca–Zn biocompatible metallic glass having small amounts of Ca (0–8 at%) has been found suitable for the development of biodegradable implants [8–10]. Since the Mg–Ca–Zn system is promising as a next-generation material in both transportation and biomedical applications, having an accurate understanding of the system is necessary.

Although the Mg–Ca–Zn ternary system and all three binary constituents have already been modeled [11,12], some binary compounds in two of the constituent binaries, Mg–Ca and Ca–Zn, and Mg–Ca–Zn ternary have been re-optimized following the availability of detailed experimental data on the Mg–Ca–Zn system by Zhang et al. [13]. The changes incorporated in the model presented in this study are given as follows: (a) Zhang et al. [13] determined the extended ternary solid solubility of $Mg_2Ca$. In the reported thermodynamic modeling of the system [11,12], $Mg_2Ca$ had been included as the compound with no ternary solubility whereas in this study, extended ternary solid solubility of $Mg_2Ca$ has been considered. (b) Zhang et al. [13] reported the ternary solubility of $CaZn_{11}$ and $CaZn_{13}$ binary compounds experimentally. In the present study, both $CaZn_{11}$ and $CaZn_{13}$ have been considered as solid solutions with respective ternary solubility unlike earlier studies [11,12]. (c) Two ternary intermetallic compounds IM1 (where IM denotes intermetallic compound) and IM3 having complex solubility ranges have been considered as solid solutions. IM2 and IM4 have been treated as the stoichiometric phases due to their very limited homogeneity range. (d) Calculated vertical section of the system in the Mg-rich region at constant Ca composition (Ca=4, 6 at%) has been compared with the experimental data of [14], where this system shows promising compositions for the formation of bulk metallic glass for biomedical applications [8]. In addition, ternary interaction parameters in the liquid phase have also been re-optimized in the present

* Corresponding author.
*E-mail address:* mmedraj@encs.concordia.ca (M. Medraj).

http://dx.doi.org/10.1016/j.calphad.2014.03.003
0364-5916/

study. Thermodynamic parameters of stoichiometric phases in the constituent binaries other than mentioned above have been taken from the literature [12]. All the binary and ternary phases with solubility ranges ($Mg_2Ca$, $CaZn_{11}$, $CaZn_{13}$, IM1 and IM3) have been modeled using compound energy formulism (CEF) and the liquid phase has been modeled with the modified quasi-chemical model.

## 2. Literature review

Experimental studies and efforts to present a consistent and accurate thermodynamic description of the Mg–Ca–Zn system and constituent binaries were undertaken in the past by different groups [11,12,15–34]. Based on the metallographic studies and cooling curves data of 189 alloys, Paris [15] reported 16 different isopleths and reported a ternary compound with the composition $Ca_2Mg_5Zn_5$. However, Paris [15] did not report any crystallographic data for this compound. Later, Clark [16] investigated the isothermal section of the Mg–Ca–Zn system at 608 K employing metallography and X-ray diffraction of 76 alloys and reported the presence of two ternary compounds $Ca_2Mg_6Zn_3$ and $Ca_2Mg_5Zn_{13}$ [17,18]. Based on the above experimental data [15–18], the thermodynamic modeling of the system was carried out by Brubaker and Liu [11] considering one ternary stoichiometric compound: $Ca_2Mg_6Zn_3$ and speculating the existence of another, $Ca_2Mg_5Zn_{13}$. But because of lack of sufficient experimental information they could not confirm the existence of the second ternary compound in the Mg–Ca–Zn system. Brubaker and Liu [11] employed the random mixing model for the liquid phase which does not take short range ordering in the liquid into account. Later on, Wasiur-Rehman and Medraj [12] re-optimized the Mg–Ca–Zn system by considering different scenarios combining the work of Paris [15] and Clark [16–18]. As a best fit to the experimental data, two ternary compounds reported by Clark [16–18] were included in the thermodynamic modeling. The isothermal sections of the Mg–Ca–Zn system at 608 K modeled by Brubaker and Liu [11] and Wasiur-Rehman and Medraj [12] are presented in Fig. 1a and b. The appearance of the additional liquid region close to the Mg–Zn side reported by Brubaker and Liu [11] is not consistent with the experimental data [15]. Recently, Zhang et al. [13] experimentally studied the isothermal section of the Mg–Ca–Zn system at 608 K using a combination of the high-throughput diffusion couple technique and equilibrated key alloys. The existence of four intermetallic ternary compounds was reported: $Ca_3Mg_xZn_{15-x}$ ($4.6 \le x \le 12$ at 608 K), $Ca_{14.5}Mg_{15.8}Zn_{69.7}$, $Ca_2Mg_5Zn_{13}$ and $Ca_{1.5}Mg_{55.3}Zn_{43.2}$, designated as IM1, IM2, IM3 and IM4 respectively. Both IM1 and IM3 show extended ternary solubility while IM2 and IM4 were reported as stoichiometric compounds [35]. The crystallographic information of the ternary and binary compounds in the Ca–Mg–Zn system is listed in Table 1 [35–37]. The structure of IM1 is hexagonal with lattice parameters $a=0.9958$ nm and $c=1.0395$ nm at 66.9 at% Mg content [35]. IM3 ternary intermetallic crystalizes in the hexagonal structure with lattice parameters $a=1.4756$ nm and $c=0.8804$ nm [36]. The homogeneity range of IM3 is $8.2 \le Ca \le 9.1$, $27.1 \le Mg \le 31.0$ and $60.8 \le Zn \le 64.7$ at 608 K [36]. In addition, Zhang et al. [13] reported extended ternary solubility for $Mg_2Ca$, $CaZn_{11}$ and $CaZn_{13}$ binary compounds. $Mg_2Ca$ has a hexagonal C14-type crystal structure with lattice parameters $a=0.62528$ nm and $c=1.01435$ nm [38] and $MgZn_2$ has lattice parameters $a=0.5220$ nm and $c=0.8566$ nm [39]. The maximum ternary solubility of $Mg_2Ca$ corresponds to $Ca_{33.3}Mg_{55.9}Zn_{10.8}$ composition.

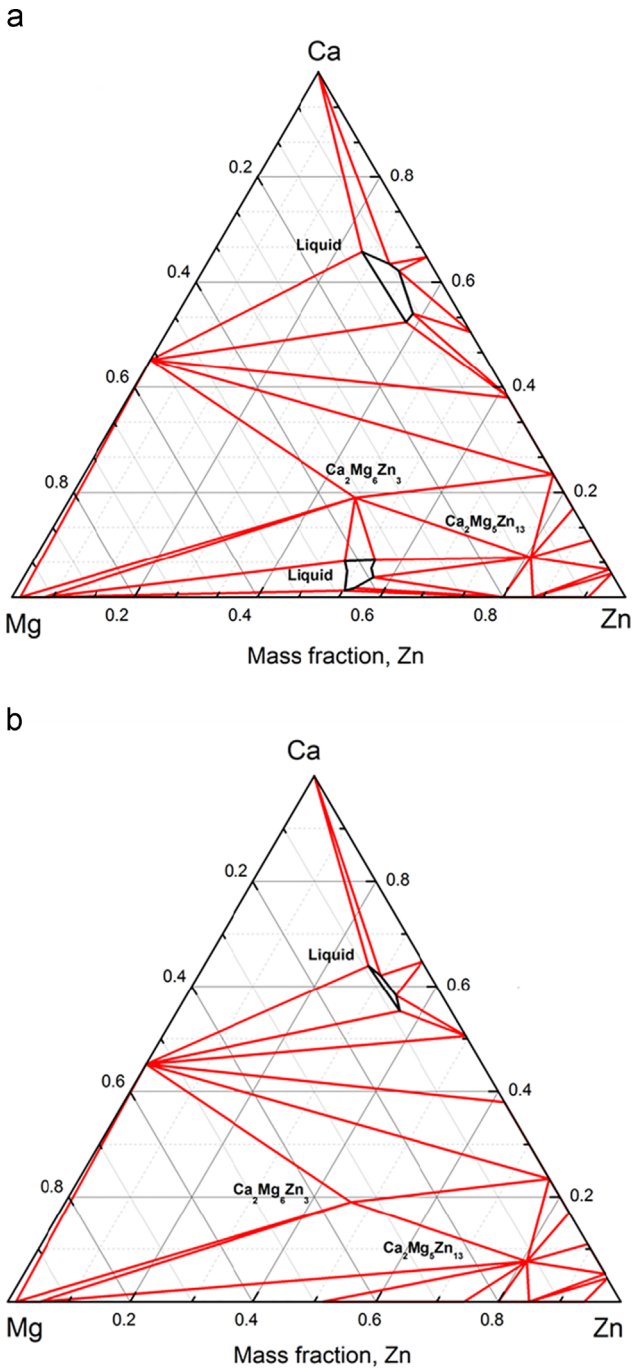


**Fig. 1.** Comparison of the 608 K isothermal section of (a) Brubakar and Liu [11]; (b) Wasiur-Rehman and Medraj [12].

**Table 1**
Crystallographic information of the ternary and binary compounds in the Ca–Mg–Zn system [35–37].

| Phase | Pearson symbol | Space group | Lattice parameters (Å) | | |
|---|---|---|---|---|---|
| | | | *a* | *b* | *c* |
| $Mg_2Ca$ | hP12 | $P6_3/mmc$ (194) | 6.253 | 6.253 | 1.014 |
| $CaZn_2$ | I12 | *Imma* (74) | 4.591 | 7.337 | 7.667 |
| $CaZn_3$ | hP32 | $P6_3/mmc$ (194) | 9.168 | 9.168 | 7.327 |
| $CaZn_5$ | hP6 | *P6/mmc* (191) | 5.371 | 5.371 | 4.242 |
| $CaZn_{11}$ | tI48 | $I4_1/amd$ *O2* (141) | 10.699 | 10.699 | 6.830 |
| $CaZn_{13}$ | cF112 | *Fm-3c* (226) | 12.154 | 12.154 | 12.154 |
| Zn | hP2 | $P6_3/mmc$ (194) | 2.665 | 2.665 | 4.947 |
| Mg | hP2 | $P6_3/mmc$ (194) | 3.199 | 3.199 | 5.154 |
| $MgZn_2$ | hP12 | $P6_3/mmc$ (194) | 5.220 | 5.220 | 8.566 |
| $Mg_2Zn_{11}$ | cP39 | *Pm-3* (200) | 8.552 | 8.552 | 8.552 |
| IM1 [35] | hP36 | $P6_3/mmc$ (194) | 9.958 | 9.958 | 1.039 |
| IM3 [36] | hP92 | $P6_3/mmc$ (194) | 14.756 | 14.756 | 8.804 |

$CaZn_{11}$ has the tetragonal crystal structure with lattice parameters $a=1.0699$ nm and $c=0.6830$ nm [40]. $CaZn_{13}$ has the fcc lattice with lattice parameter $a=1.21543$ nm [41]. $CaZn_{11}$ and $CaZn_{13}$ show the maximum ternary solubility to be 8.4 and 15.5 at% Mg, respectively. The solubility range and crystal structure of $Mg_2Ca$, $CaZn_{11}$, $CaZn_{13}$, IM1 and IM3 at 608 K were studied using scanning electron microscopy (SEM), electron probe micro-analysis (EPMA), transmission electron microscopy (TEM), electron back-scattered diffraction (EBSD) and X-ray diffraction (XRD) [13,35,36]. In addition, based on the atomic occupancy results and the crystallographic details, two sublattice models were proposed for these two ternary solid solutions [35,36]. Therefore, based on the intensive experimental data reported by our group [13,14,35,36] on the Mg–Ca–Zn system, re-optimization has been carried out in this work.

## 3. Thermodynamic models

### 3.1. Pure elements

Gibbs energy of formation of Ca, Mg and Zn of a structure $\varphi$ as a function of temperature ($T$) is described as

$$^{0}G^{\varphi}_{Ca/Mg/Zn}(T) = a + bT + cT\ln T + dT^2 + eT^3 + fT^{-1} + gT^7 + hT^{-9} \quad (1)$$

where, $^{0}G^{\varphi}_{Ca/Mg/Zn}(T)$ is the Gibbs energy at the standard state and $T$ is the absolute temperature. The values of the coefficients $a$–$h$ are taken from the SGTE (Scientific Group Thermodata Europe) compilation by Dinsdale [42].

### 3.2. Liquid phase

Several models have been proposed to thermodynamically describe the liquid phase. Binary systems such as Ca–Zn and Mg–Zn, show strong compound forming tendency and display a pronounced minimum in the enthalpy of mixing of the liquid phase. This is caused due to the presence of short range ordering in the liquid phase [43]. The random mixing model (Bragg–Williams model) does not consider short range ordering in the liquid and requires too many parameters for optimization to fit the experimental data. The Associate or Molecular model takes short range ordering in the liquid phase into account with the assumption that some molecules occupy some sites preferentially which is not physically sound [44]. Moreover, Associate or Molecular model does not correctly predict the thermodynamic properties of ternary solutions when constituent binaries show short range ordering [45]. The modified quasi-chemical model (MQM) with a pair approximation is therefore used in this study to model the liquid phase in the Mg–Ca–Zn system and the constituent binaries. The details of the MQM were explained in a series of articles by Dr. Pelton [46–48].

A brief description of MQM is given here. The energy of pair formation can be expressed by the following equation:

$$\Delta g_{AB} = \Delta g^{0}_{AB} + \sum_{i\geq 1} g^{i0}_{AB} X^{i}_{AA} + \sum_{j\geq 1} g^{0j}_{AB} X^{j}_{BB} \quad (2)$$

where, $\Delta g^{0}_{AB}$, $g^{i0}_{AB}$ and $g^{0j}_{AB}$ are the parameters of the model and can be expressed as functions of temperature. Another important aspect of the MQM is the atom to atom coordination number. The coordination number of atoms A and B can be written as $Z_A$ and $Z_B$, which can be expressed as function of composition. They can be presented by the following equations:

$$\frac{1}{Z_A} = \frac{1}{Z^{A}_{AA}}\left(\frac{2n_{AA}}{2n_{AA}+n_{AB}}\right) + \frac{1}{Z^{A}_{AB}}\left(\frac{n_{AB}}{2n_{AA}+n_{AB}}\right) \quad (3)$$

$$\frac{1}{Z_B} = \frac{1}{Z^{B}_{BB}}\left(\frac{2n_{BB}}{2n_{BB}+n_{AB}}\right) + \frac{1}{Z^{B}_{BA}}\left(\frac{n_{AB}}{2n_{BB}+n_{AB}}\right) \quad (4)$$

$n_{ij}$ is the number of moles of ($i$–$j$) pairs, $Z^{A}_{AA}$ and $Z^{A}_{AB}$ are the coordination numbers when all nearest neighbors of an A atom are A or B atom, respectively. The composition of maximum short range ordering is determined by the ratio $Z^{B}_{BA}/Z^{A}_{AB}$. Values of $Z^{A}_{AB}$ and $Z^{B}_{BA}$ are unique to the A–B binary system and should be carefully determined to fit the thermodynamic experimental data (enthalpy of mixing, activity etc.). The values of the coordination numbers as well as binary excess parameters for the liquid have been taken from Wasiur-Rahman and Medraj [12].

### 3.3. Terminal solid solution

The terminal solid solutions in the Mg–Ca–Zn system are modeled using the random solution model. The Gibbs energy is expressed as Redlich–Kister polynomial

$$G = x_i {}^{0}G_i^{\varphi} + x_j^{0}G_j^{\varphi} + RT\left[x_i\ln x_i + x_j\ln x_j\right] + {}^{ex}G_{\varphi} \quad (5)$$

where $i$ and $j$ are the elements of the binary $i$–$j$ system, $^{ex}G^{\varphi}$ is the excess Gibbs energy function expressed as

$${}^{ex}G_{\varphi} = X_iX_j\left[{}^{0}L^{\varphi}_{i,j} + (X_i - X_j)^{1}L^{\varphi}_{i,j} + (X_i - X_j)^{2}{}^{2}L^{\varphi}_{i,j}\right] \quad (6)$$

Each of the $L$ terms may be temperature dependent according to

$${}^{n}L^{\varphi}_{i,j} = a + bT \quad (7)$$

The parameters $a$ and $b$ are generated by optimization using experimental results of phase equilibria and thermodynamic data.

### 3.4. Intermediate stoichiometric compounds

Gibbs energy of the stoichiometric compounds IM2 and IM4 is described using the following expression:

$$G^{\varphi} = x_i {}^{0}G_i^{\varphi} + x_j^{0}G_j^{\varphi} + x_k^{0}G_k^{\varphi} + \Delta G^{f} \quad (8)$$

where, $\varphi$ denotes the phase of interest, $x_i$, $x_j$ and $x_k$ are the mole fraction of components $i$, $j$ and $k$ and $G_i^{\varphi}$, $G_j^{\varphi}$ and $G_k^{\varphi}$ represent the Gibbs energy of the components in their standard state and $\Delta G^{f} = a + bT$ is the Gibbs energy of formation per mole of atoms of the stoichiometric compound. The parameters $a$ and $b$ are determined in the same way to that of terminal solid solutions.

### 3.5. Intermediate solid solution phases

The Gibbs energy of intermediate solid solutions $Mg_2Ca$, $MgZn_2$, $CaZn_{11}$, $CaZn_{13}$, IM1 and IM3 in the Mg–Ca–Zn system is described by the compound energy formalism (CEF) as

$$G = G^{ref} + G^{ideal} + G^{excess}$$

$$G^{ref} = \sum y_i^{l} y_j^{m} \ldots y_k^{q}\ {}^{o}G_{(i:j:\ldots:K)} \quad (9)$$

$$G^{ideal} = RT\sum_l f_l \sum_l y_i^{l} \ln y_i^{l} \quad (10)$$

$$G^{excess} = \sum y_i^{l} y_j^{l} y_k^{m} \sum_{\gamma=0} {}^{\gamma}L_{(i,j):k}(y_i^{l} - y_j^{l})^{\gamma} \quad (11)$$

where, $i$, $j$, … $k$ represent components or vacancy in $l$, $m$ and $q$ sublattices. $y_i^{l}$ represents the site fraction of component $i$ on sublattice $l$; $f_l$ is the fraction of sublattice $l$ relative to the total lattice sites, $^{0}G_{(i,j,\ldots,k)}$ represents the compound energy of a real or a hypothetical end member in the sublattice model. $^{\gamma}L_{(i,j):k}$ represents the interaction parameters which describe the interaction between the constituents within the sublattice.

During the optimization of the model parameters, the Gibbs energy of formation of the hypothetical end members is given a

high positive value to avoid any unwanted formation whereas for the stable compounds the values are determined. Two sublattice model (Mg%, Ca, Zn)$_2$ (Mg, Ca%, Zn) is used to describe Zn solubility in $Mg_2Ca$. Here, % denotes the major constituent of the sublattice. Among all the end members, $Mg_2Ca$ and $MgZn_2$ are the stable phases and all other end members are hypothetical. This model covers the entire composition range of the system therefore the homogeneity range of $Mg_2Ca$ and $MgZn_2$ could be successfully reproduced. Based on the crystallographic information reported by Zhang et al. [35] for IM1 a three sublattice model, (Ca)(Zn, Mg)(Mg, Zn)$_4$ has been used to reproduce the solubility. The model allows the mixing of Mg and Zn in two of the lattices. It covers the composition from 0 to 83.33 at% Zn which includes the solubility range of IM1 completely. Therefore the solubility range of IM1 could be reproduced using this model. In the case of IM3, on the basis of the atomic occupancy results and the crystallographic details, Zhang et al. [36] proposed a three-sublattice model $(Ca\%)_3(Ca, Mg\%)_{13}(Mg, Zn\%)_{30}$ for this compound. The model was modified by incorporating vacancies into two of the constituent lattices as $(Ca\%, Va)_3(Ca, Mg\%, Va)_{13}(Mg, Zn\%)_{30}$. IM3 has a diffused solubility with uneven contour. Using the proposed three-sublattice model by [36], it was not possible to model the solubility of IM3 thermodynamically. Although Zhang et al. [36] analyzed all three sublattices critically and defined all the site

**Table 2**
Nominal and actual composition of the samples and the transformation temperature at different scan rates for the samples with Ca=4 at%.

| Sample No. | Nominal composition (at%) | Actual composition (at%) | Scan rate (K/min) | Transformation temperature at different scan rates (K) | |
|---|---|---|---|---|---|
| | | | | Phase transformation no.1 | Liquidus (obtained from cooling) |
| 1 | $Ca_4Mg_{68}Zn_{28}$ | $Ca_{4.1}Mg_{70.8}Zn_{25.1}$ | 10 | 611 | 641 |
| | | | 5 | 611 | 641 |
| | | | 0[a] | 611 | 641 |
| 2 | $Ca_4Mg_{66}Zn_{30}$ | $Ca_{4.2}Mg_{68.7}Zn_{27.1}$ | 10 | 611 | 619 |
| | | | 5 | 611 | 620 |
| | | | 0[a] | 611 | 621 |
| 3 | $Ca_4Mg_{64}Zn_{32}$ | $Ca_{4.3}Mg_{66.1}Zn_{29.6}$ | 10 | 611 | – |
| | | | 5 | 611 | – |
| | | | 0[a] | 611 | – |
| 4 | $Ca_4Mg_{62}Zn_{34}$ | $Ca_{4.1}Mg_{63.2}Zn_{32.7}$ | 10 | 611 | 633 |
| | | | 5 | 611 | 638 |
| | | | 0[a] | 611 | 643 |
| 5 | $Ca_4Mg_{60}Zn_{36}$ | $Ca_{3.8}Mg_{60.4}Zn_{35.8}$ | 10 | 611 | 665 |
| | | | 5 | 611 | 665 |
| | | | 0[a] | 611 | 665 |

[a] Extrapolated.

**Table 3**
Nominal and actual composition of the samples and the transformation temperature at different scan rates for the samples with Ca=6 at%.

| Sample no. | Nominal composition (at%) | Actual composition (at%) | Scan rate (K/min) | Transformation temperature at different scan rates (K) | | |
|---|---|---|---|---|---|---|
| | | | | Phase transformation no.1 | Phase transformation no.2 | Liquidus (obtained from cooling) |
| 6 | $Ca_6Mg_{72}Zn_{22}$ | $Ca_{6.1}Mg_{72.7}Zn_{21.2}$ | 10 | 611 | 647 | 686 |
| | | | 5 | 611 | 649 | 688 |
| | | | 0[a] | 611 | 651 | 690 |
| 7 | $Ca_6Mg_{70}Zn_{24}$ | $Ca_{6.2}Mg_{70.5}Zn_{23.3}$ | 10 | 611 | 641 | 669 |
| | | | 5 | 611 | 641 | 672 |
| | | | 0[a] | 611 | 641 | 675 |
| 8 | $Ca_6Mg_{68}Zn_{26}$ | $Ca_{5.8}Mg_{67.4}Zn_{26.8}$ | 10 | 611 | – | 627 |
| | | | 5 | 611 | – | 627 |
| | | | 0[a] | 611 | – | 627 |
| 9 | $Ca_6Mg_{66}Zn_{28}$ | $Ca_{6.1}Mg_{64.8}Zn_{29.1}$ | 10 | 611 | – | 627 |
| | | | 5 | 611 | – | 627 |
| | | | 0[a] | 611 | – | 627 |
| 10 | $Ca_6Mg_{64}Zn_{30}$ | $Ca_{6.0}Mg_{62.7}Zn_{31.3}$ | 10 | 611 | – | 623 |
| | | | 5 | 611 | – | 623 |
| | | | 0[a] | 611 | – | 623 |
| 11 | $Ca_6Mg_{62}Zn_{32}$ | $Ca_{5.8}Mg_{60.0}Zn_{34.2}$ | 10 | 611 | – | 654 |
| | | | 5 | 611 | – | 654 |
| | | | 0[a] | 611 | – | 654 |
| 12 | $Ca_6Mg_{60}Zn_{34}$ | $Ca_{6.2}Mg_{58.5}Zn_{35.3}$ | 10 | 611 | – | 646 |
| | | | 5 | 611 | – | 649 |
| | | | 0[a] | 611 | – | 652 |

[a] Extrapolated.

occupancies, they did not find any other anti-structure elements mixed in these lattices. Therefore vacancies are added to the first two sublattices according to the general guidelines by Hillert [49]. The occurrence of vacancy is natural in the lattices and their presence provides flexibility during modeling. Among the end members of this model, $Ca_3Mg_{13}Zn_{30}$ is close to the stability range of IM3 and hence Gibbs free energy of formation is negative and is optimized to stabilize the compound. All other end members of the model are hypothetical. This model also covers the whole composition range in which IM3 is stable or in equilibrium with other phases. As for the Ca–Zn binary compounds extending in the ternary system, $CaZn_{11}$ and $CaZn_{13}$ have been remodeled using sublattice model to accommodate the ternary solubility. The earlier assessment by [12] used stoichiometric model for these compounds since no solubility was reported at that time. $CaZn_{11}$ and $CaZn_{13}$ are modeled using two sublattices as $(Ca)(Mg, Zn)_{11}$ and $(Ca)(Mg, Zn)_{13}$, respectively, where Mg mixes in the second lattices.

## 4. Experimental procedure

To investigate the behavior of the glass formation and to confirm the consistency of the thermodynamic model with experimental

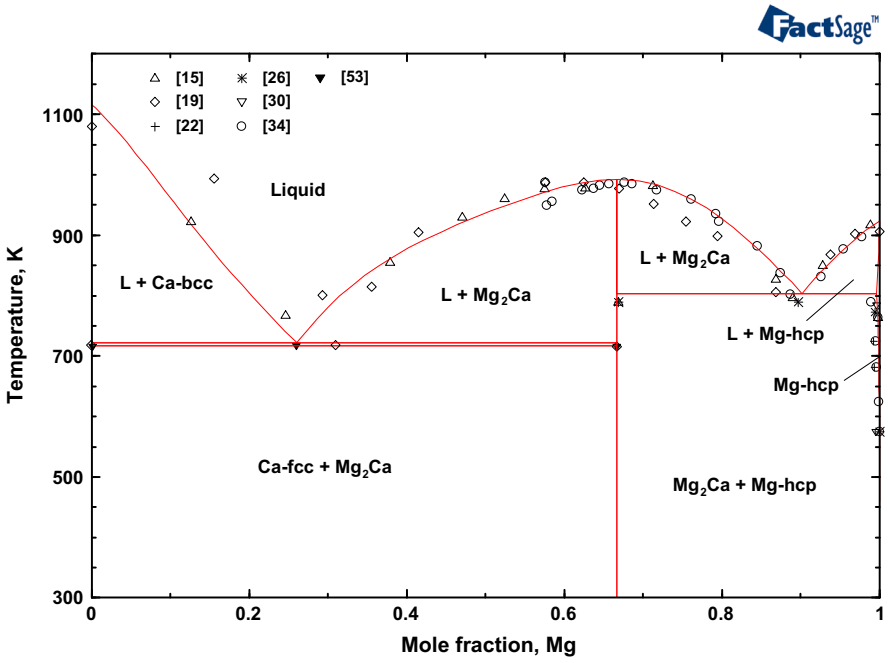


**Fig. 2.** Comparison of the optimized Mg–Ca binary phase diagram with the experimental data from literature.

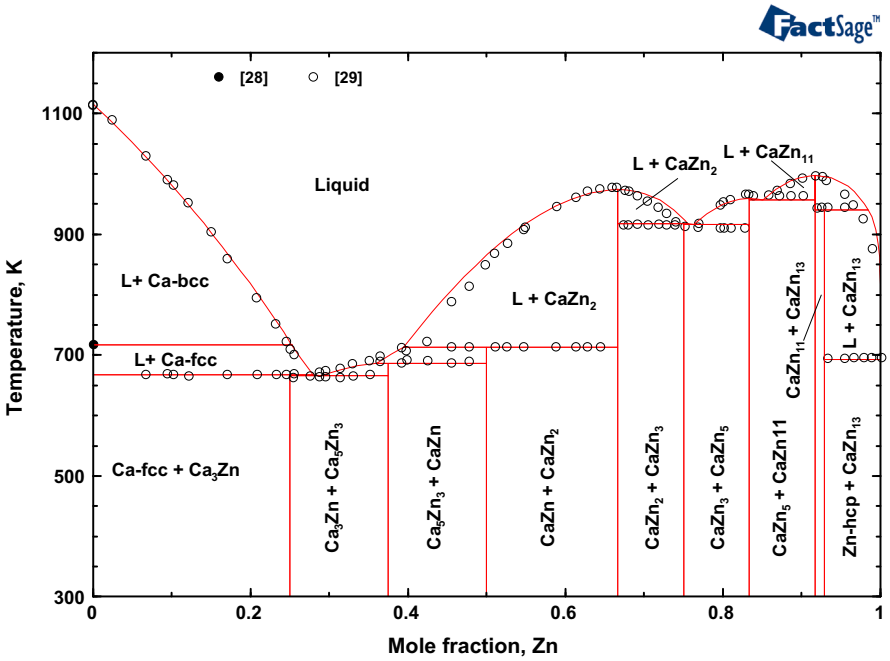


**Fig. 3.** Comparison of the optimized Ca–Zn binary phase diagram with the experimental data from literature.

results, 5 samples with 4 at% Ca and 7 samples with 6 at% Ca were prepared. The starting materials were supplied by Alfa Aesar with purities of 99.98% Mg, 99.99% Zn and 99% Ca. The alloys were prepared in an arc-melting furnace with water-cooled copper crucible in an argon atmosphere using a non-consumable tungsten electrode. Samples were re-melted five times to ensure homogeneity. To compensate for the mass loss of Mg and Zn due to their high vapor pressure, extra 8 and 12 weight percentages of Mg and Zn, respectively, were added to the compositions before melting. The actual composition of the samples was determined by Inductively Coupled Plasma (Ultima 2 ICP-OES) spectrometer. The nominal and actual compositions of the samples used in this paper are listed in Tables 2 and 3. The difference between nominal compositions and actual compositions is below 3 at%. The actual compositions were used for the analysis.

The melting temperatures and phase transformations were studied using 5 and 10 K/min heating and cooling rates by means of a differential scanning calorimeter (DSC) from SETARAM Instrumentation under a continuous flow of purified argon. Temperature calibration of the DSC equipment was done using standard samples of Sn, Al, Zn, Ni and Au. Samples were placed in a graphite crucible covered with a lid. The reproducibility of every measurement was confirmed by collecting the data during three different heating and cooling cycles on each sample. The estimated error of measurements between the repetitive cycles is $\pm 2$ K or less. Temperatures corresponding to various thermal events were obtained from the analysis of the DSC curves during heating and cooling runs. As mentioned earlier, the alloys were prepared in an arc melting furnace. During melting the temperature of the furnace reaches more than 3200 K. While in the DSC experiments, the temperature is kept around 775 K. Thus the mass loss/oxidation was not a concern during the DSC experiments as it was during the arc-melting. However, Thermo-gravimetric analysis (TGA) was done to observe any mass loss or gain of the samples

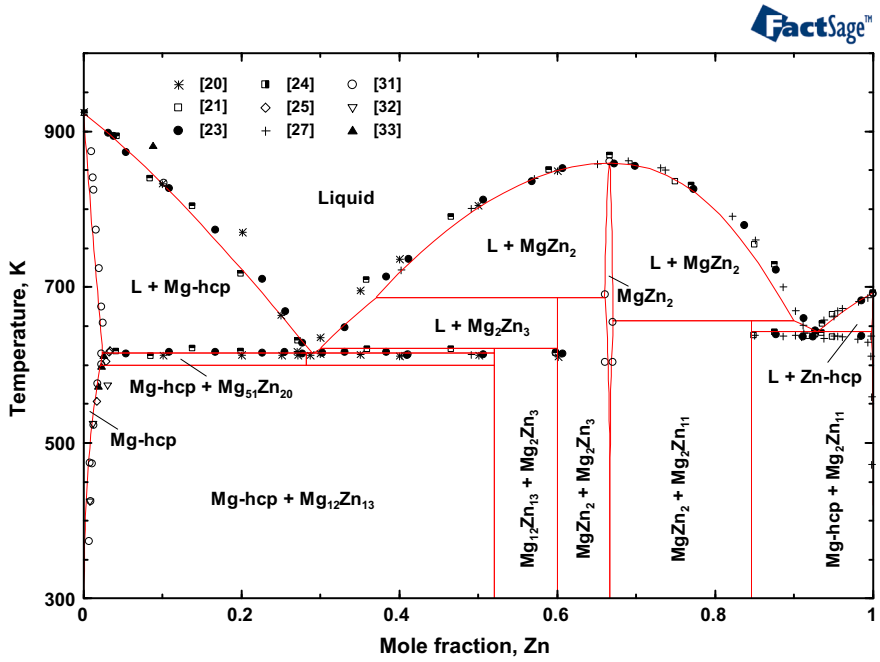


**Fig. 4.** Comparison of the optimized Mg–Zn binary phase diagram with the experimental data from literature.

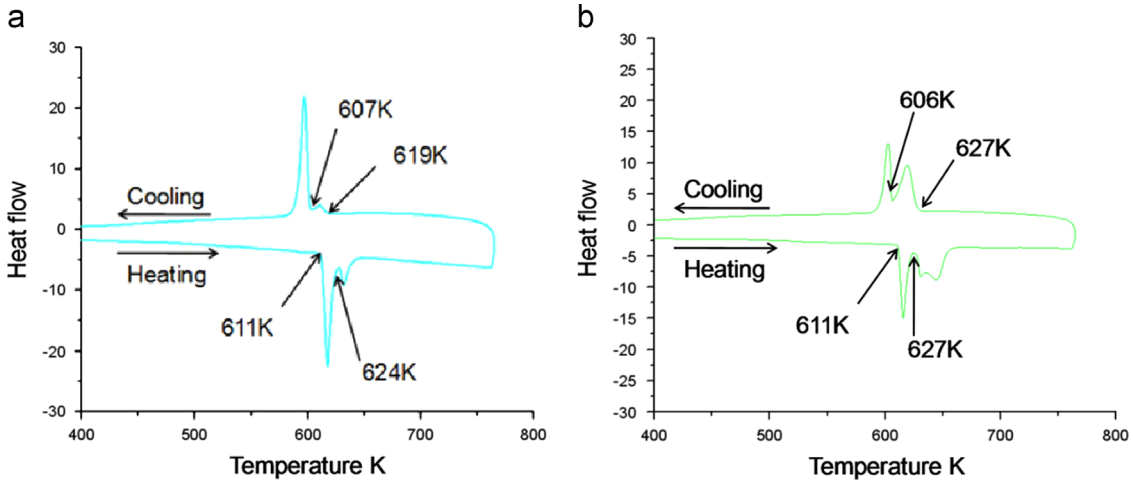


**Fig. 5.** DSC curve with the heating and cooling rate 10 K/min (a) sample no. 2 ($Ca_{4.2}Mg_{68.7}Zn_{27.1}$) containing 4 at% Ca and (b) sample no. 8 ($Ca_{5.8}Mg_{67.4}Zn_{26.8}$) containing 6 at % Ca.

due to decomposition or oxidation. None of the DSC measurements showed fluctuation in the TGA curve during the experiments. Also, each sample was weighed and inspected visually before and after the experiment to detect any change in mass or discoloration due to oxidation.

## 5. Results and discussion

### 5.1. The constituent binaries of the Mg–Ca–Zn system

The calculated Mg–Ca phase diagram using the current database has been compared with the experimental data from the literature [15,19,22,26,30,34,50] as shown in Fig. 2. Recently, it has been reported that $Mg_2Ca$ has ternary solubility in the Mg–Ca–Zn system. In order to incorporate the solubility of Zn in $Mg_2Ca$, it has been re-optimized using a two Sublattice model which has been discussed earlier in Section 3.5. In addition, the ternary solid solubility in the $MgZn_2$ binary compound is negligible. $Mg_2Ca$ and $MgZn_2$ being iso-structural compounds, Laves_C14 phase, have been modeled by CEF employing the same Gibbs energy function in the Mg–Ca–Zn ternary system. The optimized Ca–Zn binary phase diagram incorporating $CaZn_{11}$ and $CaZn_{13}$ as solid solutions with Mg maintains good agreement between the optimized phase diagram and the experimental results from the literature [28,29] as shown in Fig. 3. The calculated congruent melting temperature of $CaZn_{11}$ is 996 K which matches well with the experimental value 995 K. The calculated decomposition

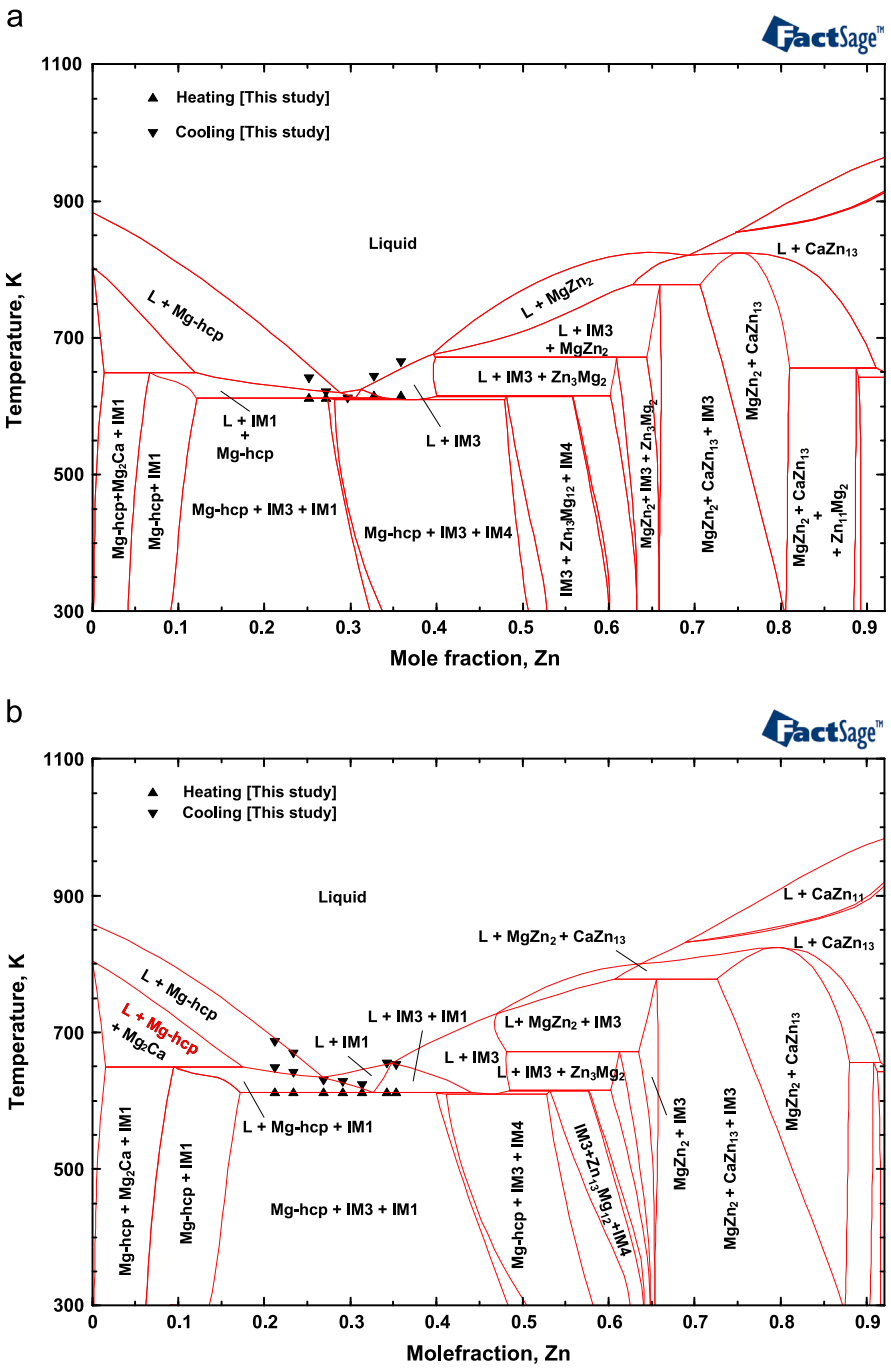


**Fig. 6.** (a) Calculated isopleths in Mg–Ca–Zn system at Ca=4 at% in comparision to the experimental data. (b) Calculated isopleths in Mg–Ca–Zn system at Ca=6 at% in comparision to the experimental data.

temperature of $CaZn_{13}$, 940 K, is close to the experimental value 944 K. The calculated Mg–Zn phase diagram with the experimental data from the literature [20,21,23–25,27,31–33] is presented in Fig. 4. The calculated congruent melting temperature and binary homogeneity range of $MgZn_2$ are found to be in good agreement with the available experimental data from the literature. During optimization the model parameters of the binary liquid and stoichiometric compounds were taken from an earlier work [12] of our group to ensure the consistency with the available experimental phase diagram and thermodynamic properties.

### 5.2. Mg–Ca–Zn system

A complete self-consistent thermodynamic database for the Mg–Ca–Zn system has been constructed. Unlike Brubaker and Liu [11], Wasiur-Rehman and Medraj [12], four ternary intermetallic compounds, IM1, IM2, IM3, IM4 reported by Zhang et al. [13] are included in the modeling. Since all the binaries show similar thermodynamic properties and do not differ to a large extent, symmetric Kohler geometric model [51] was employed for the extrapolation into the ternary system. Three ternary interaction parameters for the liquid phase have been used to achieve consistency with the current and literature experimental results.

#### 5.2.1. Vertical section from this study

Fig. 5a and b shows the DSC curves of samples 2 and 8. In sample 2, two peaks can be observed in both heating and cooling cycles. At 10 K/min scan rate, onset of the heating peaks is found at 611 K and 626 K, which are encountered at 607 K and 619 K during cooling. The difference between onset of heating and onset of cooling of liquidus indicates noticeable super cooling effect where the liquidus temperature during heating was found to be 626 K while 619 K during cooling. Therefore the correct liquidus temperature of this sample should be somewhere in between these two values. In order to minimize the super cooling effect, DSC measurements at 5 and 10 K/min are extrapolated to 0 K/min i.e. to the equilibrium, as shown in Table 2. Hence, the corrected liquidus temperature during heating and cooling are obtained as 624 K and 621 K, respectively. The experimental data along with vertical sections at 4 at% and 6 at% Ca from this study have been compared with the current thermodynamic calculations as shown in Fig. 6a and b. The calculated vertical sections fit very well with the experimental data. The presence of deep eutectic indicates the high potential for the formation of metallic glasses, which is in agreement with our previous findings [14].

#### 5.2.2. Vertical section from the literature

Different vertical sections calculated in the present study have been compared with the experimental results of Paris [15] as shown

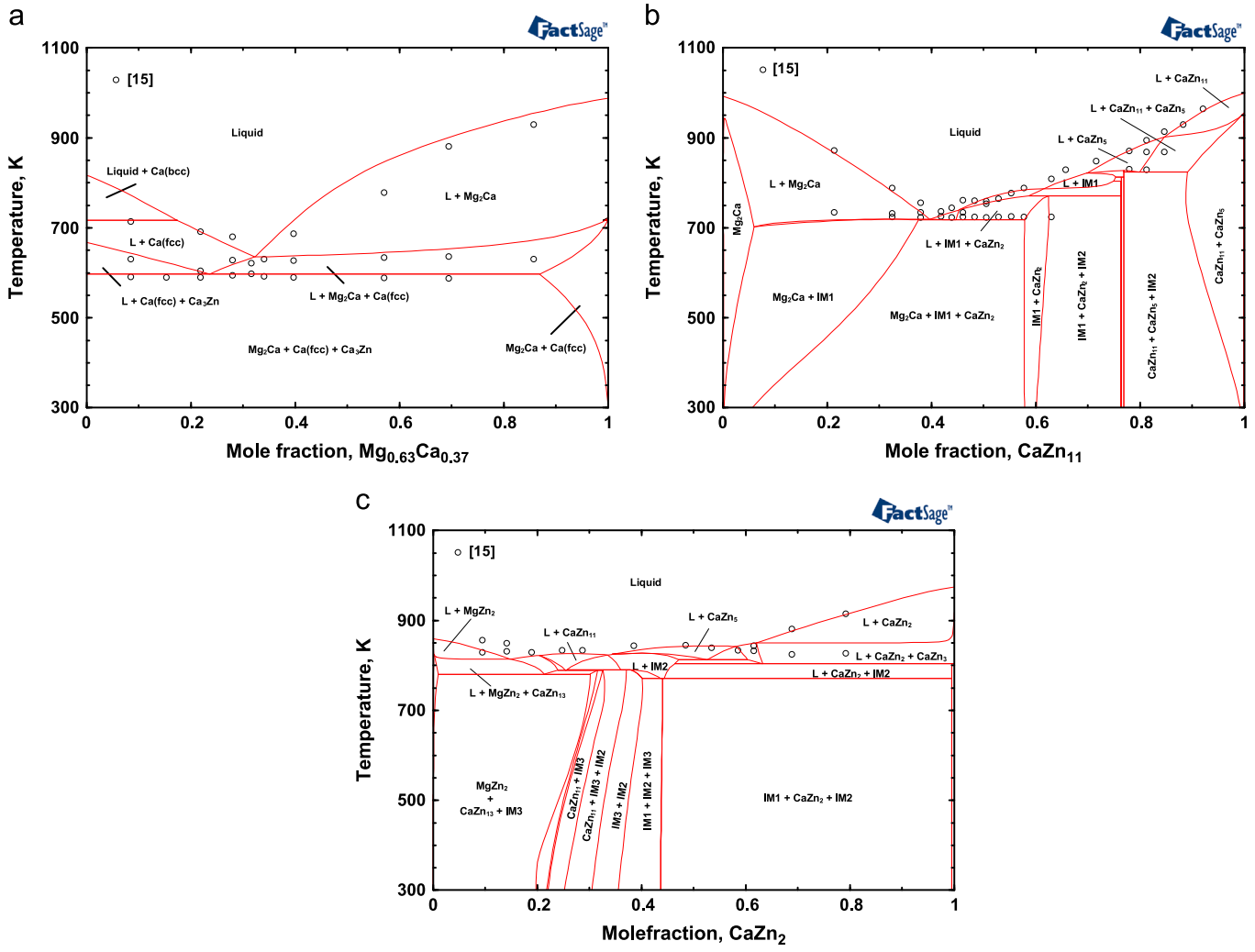


**Fig. 7.** (a) Calculated isopleth between $Mg_{0.63}Ca_{0.37}$–$Ca_{0.80}Zn_{0.20}$ in Mg–Ca–Zn system in comparision to the experimental data. (b) Calculated isopleth $Mg_2Ca$–$CaZn_{11}$ in Mg–Ca–Zn system in comparision to the experimental data. (c) Calculated isopleth $MgZn_2$9$CaZn_2$ in Mg–Ca–Zn system in comparision to the experimental data.

in Fig. 7a–c. Vertical sections along $Mg_{0.63}Ca_{0.37}$–$Ca_{0.80}Zn_{0.20}$, $Mg_2Ca$–$CaZn_{11}$ and $MgZn_2$–$CaZn_2$ are plotted in Fig. 7a–c. Fig. 7a shows the agreement between the calculated vertical section and the experimental data of Paris [15] and demonstrates the accuracy of the current thermodynamic model. The vertical sections shown in Fig. 7b and c along the composition range $Mg_2Ca$–$CaZn_{11}$ and $MgZn_2$–$CaZn_2$ represent the complex Zn-rich corner of the Mg–Ca–Zn system and are consistent with the experimental data of Paris [15] within the experimental error of $\pm 10$ K. Brubaker and Liu [11] presented vertical section along the composition range $Mg_2Ca$–$MgZn_2$ in comparison with the experimental data of Paris [15]. Presence of deep liquidus in the vertical section calculated from their model indicated flaw in the model. The liquidus obtained in the present study is consistent with the experimental data. Although the problem of the deep liquidus was resolved by Wasiur-Rehman and Medraj [12], their model had some issues. For example the difference between the calculated and experimental liquidus along Zn rich corner varies from ~20 to 100 K because they did not consider the presence of all the ternary compounds and the ternary solubility of the binary compounds. In the present study, the difference between the calculated and experimental phase boundaries is within $\pm 17$ K and therefore is more accurate than earlier studies [11,12].

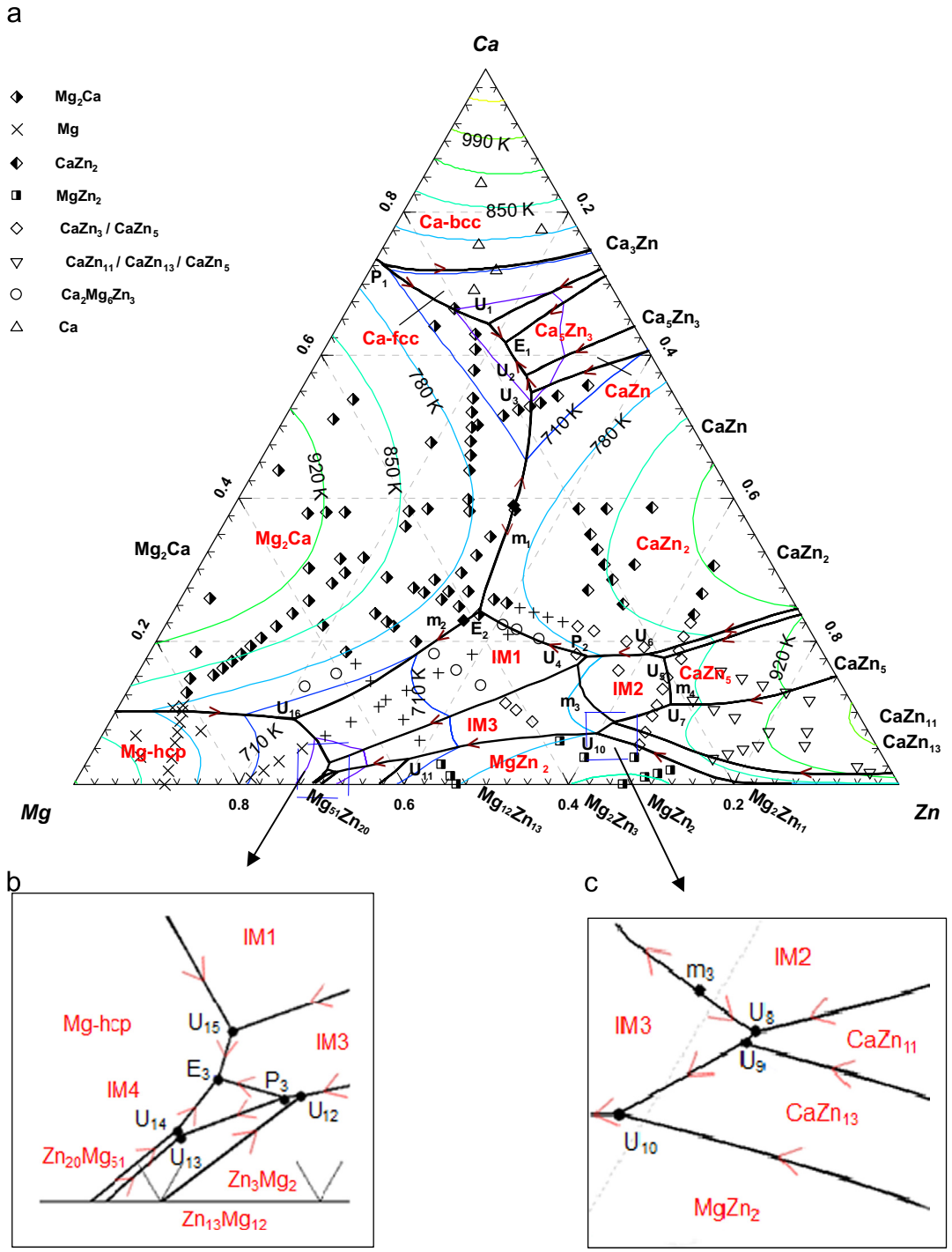


**Fig. 8.** (a) Calculated liquidus projection of the Mg–Ca–Zn system in comparision to the data from the literature [15]; (b) magnified liquidus projection near the promissing glass forming region; and (c) magnified liquidus projection near the Zn-rich region.

## 6. Liquidus projection

Fig. 8a presents the liquidus projection of the Mg–Ca–Zn system calculated in this study. The superimposed experimental data points corresponding to the primary solidification region are taken from Paris [15]. A magnified image of the promising glass forming region of the Mg–Ca–Zn system is presented in Fig. 8b. Another magnified image near the Zn-rich corner is shown in Fig. 8c to elaborate the liquidus valley. Different symbols represent different primary phases forming during solidification reported by Paris [15]. 22 invariant reactions and three maximum points are identified and their details are presented in Table 4. Liquidus projection in the system shows 20 primary crystallization regions. Four of them belong to ternary intermetallic compounds (IM1, IM2, IM3 and IM4), three to the end members (Mg-hcp, Ca-bcc and Ca-fcc) and the rest to the binary compounds. There is a good agreement between the calculated primary crystallization regions and experimental data of Paris [15] over almost the entire composition range. However, disagreement with the results of Paris [15] can be seen along the Zn-rich corner and the ternary compounds IM1, IM2, IM3. This is mainly because of difference between the nomenclatures of the compounds in these regions as Paris [15] was not aware of the existence of $CaZn_3$, $CaZn_{13}$ and different ternary intermetallic compounds IM1, IM2 and IM3. Therefore, it was not possible for him to differentiate between data for $CaZn_3$ and $CaZn_5$, $CaZn_{11}$ and $CaZn_{13}$ and ternary compounds. Hence he used the same symbol to represent the experimental data in the primary solidification regions of these phases as shown in Fig. 8a. The primary solidification region of these ternary compounds IM1 and IM3 falls under the solidification region of $Ca_2Mg_5Zn_5$, the only ternary compound Paris reported [15]. The liquidus projection for two ternary compounds reported by Brubaker and Liu [11] matches well with the results from this study except along the primary solidification region of $Ca_2Mg_5Zn_{13}$ and Zn-rich region of the ternary system. The disagreement along the primary solidification region of $Ca_2Mg_5Zn_{13}$ is due to the reason that Brubakar and Liu [11] included only two ternary compounds whereas four ternary compounds are included in the present study. In comparison with the liquidus projection reported by Wasiur-Rehman and Medraj [12], the disagreement is also along the primary solidification region of the ternary compounds. This is again due to the number of ternary compounds included in the modeling. Liquidus projection calculated in this study shows the solidification of two intermetallic compounds IM1 and IM3 in the region where Wasiur-Rehman and Medraj [12] reported the solidification of $Ca_2Mg_6Zn_3$.

## 7. Isothermal section of the Mg–Ca–Zn system

$Mg_2Ca$ shows complex ternary solubility range. Present calculation shows the solubility limit of $Mg_2Ca$ to be 3.2 at% Zn at 30.6 at% Ca which agrees well with the experimental data of Zhang et al. [13]. The other Laves phase, $MgZn_2$ does not show any ternary solubility in the Mg–Ca–Zn system. As shown in Fig. 9a and b, optimized Laves phase matches well with the experimental solubility range. The optimized model parameters of the Laves_C14 phase are presented in Table 5. Four interaction terms were necessary to reproduce the solubility range of this phase. The other binary compounds optimized in this study are $CaZn_{11}$ and $CaZn_{13}$. These compounds form substitutional solid solutions where Mg substitutes Zn. Two excess Gibbs energy parameters have been used to reproduce the solubility range of $CaZn_{13}$ whereas one is used for $CaZn_{11}$. The optimized model parameters are presented in Table 5. The solubility limits of $CaZn_{11}$ and $CaZn_{13}$, at 608 K obtained in this work are in agreement with the experimental data reported by Zhang et al. [13] within the experimental error, as shown in Fig. 9a and b.

The thermodynamic data of the ternary stoichiometric compounds, IM2 and IM4 is given in Table 6. The calculated decomposition temperature of IM2 and IM4 from this optimization is 822 K and 612 K, respectively and these compounds are stable

**Table 4**
Four-phase equilibrium points and their reactions in the Ca–Mg–Zn system.

| Equilibrium reactions | Type | Composition (at%) | | | Temp. (K) |
|---|---|---|---|---|---|
| | | Ca | Mg | Zn | |
| $L+lave\_14(Mg_2Ca)+Ca(bcc)\leftrightarrow Ca(fcc)$ | P1 | 73.08 | 25.52 | 1.40 | 716.03 |
| $L+Zn_2Ca+IM2\leftrightarrow IM1$ | P2 | 17.90 | 28.75 | 53.35 | 768.74 |
| $L+IM3+Zn_{13}Mg_{12}\leftrightarrow IM4$ | P3 | 1.91 | 67.09 | 31.00 | 613.81 |
| $L+Zn_3Ca_5\leftrightarrow ZnCa_3+lave\_14(Mg_2Ca)$ | U1 | 62.34 | 15.93 | 21.73 | 599.20 |
| $L+CaZn\leftrightarrow Zn_3Ca_5+lave\_14(Mg_2Ca)$ | U2 | 57.68 | 15.70 | 26.62 | 614.26 |
| $L+Zn_2Ca\leftrightarrow CaZn+lave\_14(Mg_2Ca)$ | U3 | 55.30 | 16.18 | 28.51 | 629.66 |
| $L+IM2\leftrightarrow IM1+IM3$ | U4 | 16.64 | 30.55 | 52.81 | 768.63 |
| $L+Zn_3Ca\leftrightarrow Zn_2Ca+IM2$ | U5 | 18.02 | 22.14 | 59.84 | 797.88 |
| $L+Zn_5Ca\leftrightarrow Zn_3Ca+IM2$ | U6 | 17.62 | 20.30 | 62.08 | 807.30 |
| $L+Zn_5Ca\leftrightarrow CaZn_{11}+IM2$ | U7 | 11.22 | 22.49 | 66.29 | 819.23 |
| $L+IM2\leftrightarrow CaZn_{11}+IM3$ | U8 | 8.84 | 30.15 | 61.01 | 787.12 |
| $L+CaZn_{11}\leftrightarrow CaZn_{13}+IM3$ | U9 | 8.62 | 30.48 | 60.90 | 786.21 |
| $L+CaZn_{13}\leftrightarrow IM3+lave\_14(MgZn_2)$ | U10 | 7.20 | 33.29 | 59.51 | 777.43 |
| $L+lave\_14(MgZn_2)\leftrightarrow IM3+Zn_3Mg_2$ | U11 | 3.77 | 57.35 | 38.88 | 670.75 |
| $L+Zn_3Mg_2\leftrightarrow IM3+Zn_{13}Mg_{12}$ | U12 | 1.94 | 66.83 | 31.23 | 615.34 |
| $L+Zn_{13}Mg_{12}\leftrightarrow IM4+Zn_{20}Mg_{51}$ | U13 | 1.20 | 69.07 | 29.72 | 609.96 |
| $L+Zn_{20}Mg_{51}\leftrightarrow IM4+Mg\text{-}hcp$ | U14 | 1.31 | 69.08 | 29.61 | 609.53 |
| $L+IM1\leftrightarrow IM3+Mg\text{-}hcp$ | U15 | 3.13 | 67.31 | 29.56 | 611.00 |
| $L+lave\_14(Mg_2Ca)\leftrightarrow IM1+Mg\text{-}hcp$ | U16 | 8.30 | 67.94 | 23.76 | 649.22 |
| $L\leftrightarrow lave\_14(Mg_2Ca)+Ca(fcc)+ZnCa_3$ | E1 | 64.94 | 16.64 | 18.41 | 600.02 |
| $L\leftrightarrow IM1+Zn_2Ca+lave\_14(Mg_2Ca)$ | E2 | 23.74 | 38.22 | 38.04 | 720.21 |
| $L\leftrightarrow Mg\text{-}hcp+IM3+IM4$ | E3 | 2.27 | 67.96 | 29.77 | 608.65 |
| $L\leftrightarrow lave\_14(Mg_2Ca)+Zn_2Ca$ | M1 | 32.95 | 31.11 | 35.94 | 753.21 |
| $L\leftrightarrow IM2+IM3$ | M2 | 9.67 | 30.70 | 59.63 | 787.74 |
| $L\leftrightarrow IM2+Zn_5Ca$ | M3 | 12.93 | 21.83 | 65.23 | 821.90 |

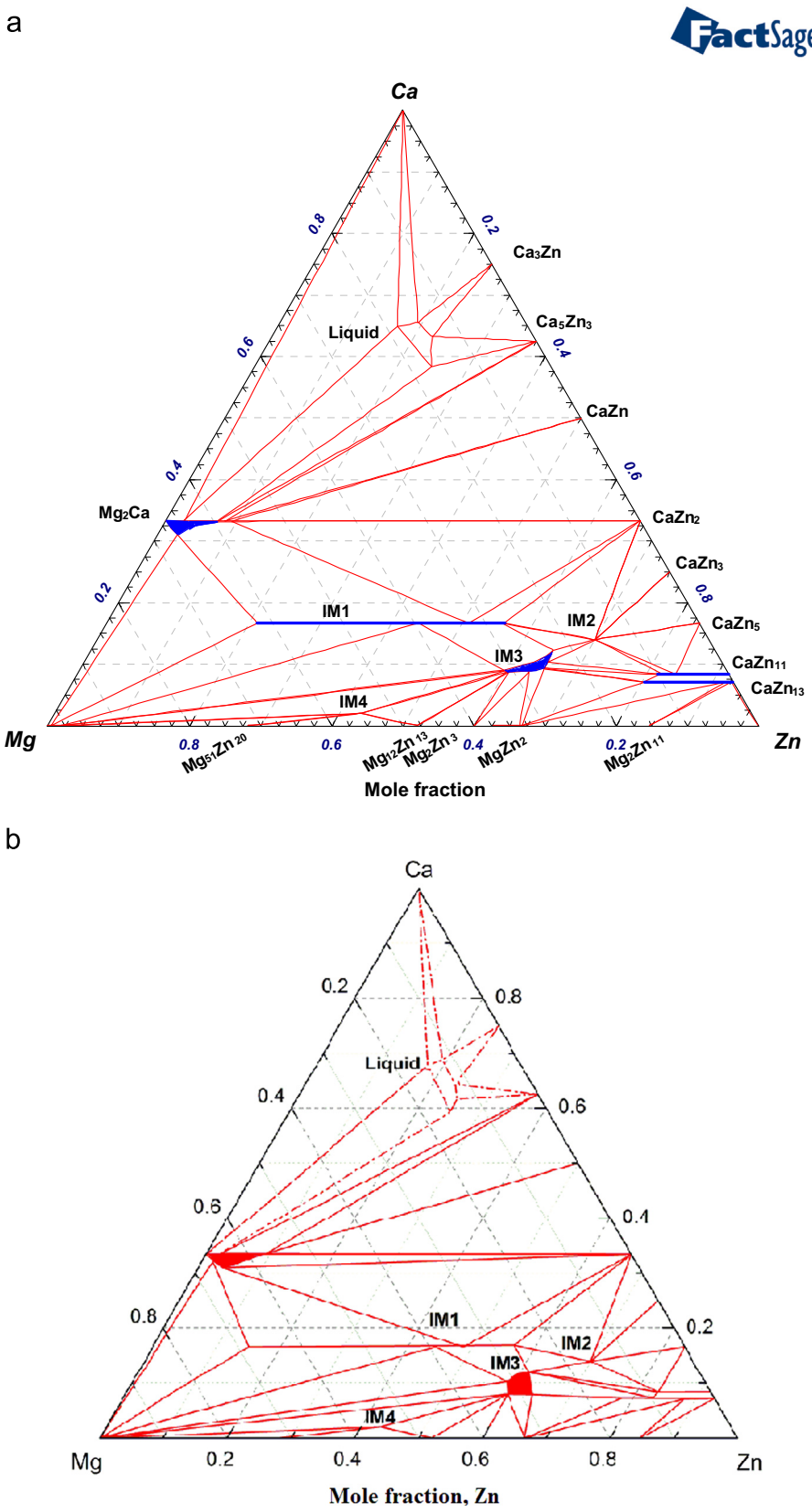


**Fig. 9.** The comparison of isothermal sections for the Mg–Ca–Zn system at 608 K (a) thermodynamic modeling optimized in this study; and (b) experimental results reported by Zhang et al. [13,35,36].

down to the room temperature. The optimized solubility range of the other two ternary compounds, IM1 and IM3 is compared with the experimental values in Fig. 9a and b. IM1 forms a substitutional solid solution in which Mg replaces Zn. Three sublattices model based on the crystallographic information of Zhang et al. [35] has been employed to model ternary intermetallic

**Table 5**
Optimized model parameters for IM1, IM3, $CaZn_{11}$, $CaZn_{13}$ and Laves_C14.

| | | |
|---|---|---|
| **IM1** | **Model: (Ca)(Zn, Mg)(Mg, Zn)$_4$** (J/mol atom) | |
| | $G_{Ca:Zn:Mg} = 1/6G$ (Ca, bcc-A2) + $1/6G$ (Zn, hcp-Zn) + $4/6G$ (Mg, hcp-A3) − 14,321.30 + 5.31$T$ | This study |
| | $G_{Ca:Zn:Zn} = 1/6G$ (Ca, bcc-A2) + $5/6G$ (Zn, hcp-Zn) − 3488.17 + 0.70$T$ | |
| | $G_{Ca:Mg:Mg} = 1/6G$ (Ca, bcc-A2) + $5/6G$ (Mg, hcp-A3) − 3488.17 + 0.70$T$ | |
| | $G_{Ca:Mg:Zn} = 1/6G$ (Ca, bcc-A2) + $4/6G$ (Zn, hcp-Zn) + $1/6G$(Mg, hcp-A3) − 19,915.34 + 7.54$T$ | |
| | $L^0_{Ca:Zn:Mg,Zn} = -47{,}997.17 + 20.79T$; $L^1_{Ca:Zn:Mg,Zn} = -17{,}650.12 + 4.88T$ | |
| | $L^0_{Ca:Zn:Zn,Mg} = 209.29 + 2.09T$; $L^1_{Ca:Zn:Zn,Mg} = -20{,}580.18 + 5.93T$; | |
| | $L^2_{Ca:Zn:Zn,Mg} = -13{,}809.65 + 1.40T$ | |
| **IM3** | **Model: (Ca, Va)$_3$(Ca, Mg, Va)$_{13}$(Mg, Zn)$_{30}$** (J/mol atom) | |
| | ${}^0G_{Ca:Ca:Mg} = 16/46G$ (Ca, bcc-A2) + $30/46G$ (Mg, hcp-A3) + 4549.78 | This study |
| | ${}^0G_{Ca:Ca:Zn} = 16/46G$ (Ca, bcc-A2) + $30/46G$ (Zn, hcp-Zn) + 3184.85 | |
| | ${}^0G_{Ca:Mg:Mg} = 3/46G$ (Ca, bcc-A2) + $43/46G$ (Mg, hcp-A3) + 5459.74 | |
| | ${}^0G_{Ca:Mg:Zn} = 3/46G$ (Ca, bcc-A2) + $13/46G$ (Mg, hcp-A3) + $30/46G$ (Zn, hcp-Zn) − 19,722.26 + 9.33$T$ | |
| | ${}^0G_{Ca:Va:Mg} = 3/46G$ (Ca, bcc-A2) + $30/46G$ (Mg, hcp-A3) + 8190.00 | |
| | ${}^0G_{Ca:Va:Zn} = 3/46G$ (Ca, bcc-A2) + $30/46G$ (Zn, hcp-Zn) + 8190.00 | |
| | ${}^0G_{Va:Ca:Mg} = 13/46G$ (Ca, bcc-A2) + $30/46G$ (Mg, hcp-A3) + 8190.00 | |
| | ${}^0G_{Va:Ca:Zn} = 13/46G$ (Ca, hcp-A2) + $30/46G$ (Zn, hcp-Zn) + 8190.00 | |
| | ${}^0G_{Va:Mg:Mg} = 43/46G$ (Mg, hcp-A3) + 8190.00 | |
| | ${}^0G_{Va:Mg:Zn} = 13/46G$ (Mg, hcp-A3) + $30/46G$ (Zn, hcp-Zn) + 8190.00 | |
| | ${}^0G_{Va:Va:Mg} = 30/46G$ (Mg, hcp-A3) + 8190.00 | |
| | ${}^0G_{Va:Va:Zn} = 30/46G$ (Zn, hcp-Zn) + 8190.00 | |
| | $L^0_{Ca,Va:Mg:Zn} = -9099.56$ | |
| | $L^0_{Ca:Ca,Mg:Zn} = L^0_{Va:Ca,Mg:Zn} = -38{,}081.68$ | |
| | $L^0_{Ca:Mg:Mg,Zn} = -2729.57$ | |
| **$CaZn_{11}$** | **Model: (Ca)(Zn,Mg)$_{11}$** (J/mol atom) | |
| | ${}^0G_{Ca:Zn} = 1/12G$ (Ca, bcc-A2) + $11/12G$ (Zn, hcp-Zn) − 14,939.82 + 3.79$T$ | This study |
| | ${}^0G_{Ca:Mg} = 1/12G$ (Ca, bcc-A2) + $11/12G$ (Mg, hcp-A3) − 978.08 + 13.26$T$ | |
| | ${}^0L_{Ca:Zn,Mg} = -22{,}533.56$ | |
| **$CaZn_{13}$** | **Model: (Ca)(Zn,Mg)$_{13}$** (J/mol atom) | |
| | ${}^0G_{Ca:Zn} = 1/14G$ (Ca, bcc-A2) + $13/14G$ (Zn, hcp-Zn) − 14,046.29 + 4.14$T$ | This study |
| | ${}^0G_{Ca:Mg} = 1/14G$ (Ca, bcc-A2) + $13/14G$ (Mg, hcp-A3) + 9988.52 + 7.18$T$ | |
| | ${}^0L_{Ca:Zn,Mg} = -36{,}715.45 + 2.24T$; ${}^1L_{Ca:Zn,Mg} = -3737.32$ | |
| **Laves_C14** | **($MgZn_2$ type): (Mg, Ca, Zn)$_2$ (Mg, Ca, Zn)** (J/mol atom) | |
| | ${}^0G_{Ca:Ca} = G$ (Ca, bcc-A2) + 42,078.60 | [12] |
| | $G_{Mg:Mg} = G$ (Mg, hcp-A3) + 3884.60 | [12] |
| | ${}^0G_{Zn:Zn} = G$ (Zn, hcp-Zn) + 7507.30 | [12] |
| | ${}^0G_{Zn:Mg} = 2/3G$ (Zn, hcp) + $1/3G$ (Mg, hcp-A3) − 11,096.56 + 0.78$T$ | This study |
| | ${}^0G_{Mg:Ca} = 2/3G$ (Mg, hcp-A3) + $1/3G$ (Ca, bcc-A2) − 16,554.68 + 3.52$T$ | This study |
| | ${}^0G_{Zn:Ca} = 2/3G$ (Zn, hcp) + $1/3G$ (Ca, bcc-A2) − 15,325.61 | This study |
| | ${}^0G_{Mg:Zn} = 2/3G$ (Mg, hcp-A3) + $1/3G$ (Zn, hcp-Zn) + 21,789.88 | This study |
| | ${}^0G_{Ca:Mg} = 2/3G$ (Ca, bcc-A2) + $1/3G$ (Mg, hcp-A3) + 5573.30 | [12] |
| | ${}^0G_{Ca:Zn} = 2/3G$ (Ca, bcc-A2) + $G$ (Zn, hcp) + 19,533.73 | This study |
| | $L^0_{Mg,Ca:Mg} = L^0_{Mg,Ca:Ca} = L^0_{Mg:Mg,Ca} = L^0_{Ca:Mg,Ca} = 14{,}006.00$ | [12] |
| | $L^0_{Mg,Zn:Mg} = L^0_{Mg,Zn:Zn} = 11{,}288.00$ | [12] |
| | $L^0_{Mg:Mg,Zn} = L^0_{Zn:Mg,Zn} = 1.40$ | [12] |
| | $L^0_{Mg:Ca,Zn} = -29{,}300.60$ | This study |

compound IM1 as discussed earlier in this paper. The compound required five interaction parameters to achieve consistency with the experimental homogeneity range. The optimized model parameters are presented in Table 5. The phase relations and homogeneity range compares well with the experimental results of [13]. IM1 is in equilibrium with Mg-hcp, $Mg_2Ca$, $CaZn_2$, IM2 and IM3 by forming five 2-phase and five 3-phase regions at 608 K. The model used for IM3 is (Ca%, Va)$_3$(Ca, Mg%, Va)$_{13}$(Mg, Zn%)$_{30}$. The optimized model parameters of IM3 are presented in Table 5. The optimized homogeneity range and phase relations agree well with the experimental data. The calculated homogeneity range of IM3 matches with the values of the experimental homogeneity range within the experimental error limit of $\pm 2$ at%. Three interaction parameters have been used for optimizing the homogeneity range of IM3. Ternary interaction parameters of the Mg–Ca–Zn liquid phase have been re-optimized using the modified quasi-chemical model in the present study. The values of the ternary interaction parameters do not have any bearing on binary phase diagrams and were kept as small as possible as suggested by Chartrand and Pelton [52]. The optimized model parameters for the liquid phase are given in Table 6. Combining the models for $Mg_2Ca$, $MgZn_2$, $CaZn_{11}$, $CaZn_{13}$, IM1 to IM4 and liquid, the re-optimized Mg–Ca–Zn isothermal section at 608 K is shown in Fig. 9a. Fig. 9b shows the experimentally determined isothermal section for this system at the same temperature by Zhang et al. [13]. The optimized isothermal section reproduces the experimental data for the

**Table 6**
Optimized model parameters for liquid and stoichiometric compounds.

| **Liquid phase** (J/mol) | | | | | **Ref.** |
|---|---|---|---|---|---|
| $Z^{Mg}_{MgCa}=5,\ Z^{Ca}_{MgCa}=4$<br>$\Delta g^{0}_{MgCa}=13,187.78+7.98T;\ \Delta g^{10}_{MgCa}=6908.55-13.0T;\ \Delta g^{01}_{MgCa}=8899.22-15.93T$ | | | | | [12] |
| $Z^{Mg}_{MgZn}=6,\ Z^{Ca}_{MgZn}=4$<br>$\Delta g^{0}_{MgZn}=-8329.74+3.19T;\ \Delta g^{10}_{MgZn}=-146.50-3.56;\ \Delta g^{01}_{MgZn}=-79.53-3.98T$ | | | | | [12] |
| $Z^{Ca}_{CaZn}=6,\ Z^{Zn}_{CaZn}=3$<br>$\Delta g^{0}_{CaZn}=-17,789.65+0.08T;\ \Delta g^{10}_{CaZn}=-10,297.07;\ \Delta g^{01}_{CaZn}=-7953.02$ | | | | | [12] |
| $\Delta g^{011}_{MgCa(Zn)}=-26,789.12;\ \Delta g^{011}_{MgZn(Ca)}=-19,254.68;\ \Delta g^{011}_{CaZn(Mg)}=-24,905.51$ | | | | | This study |
| **Mg-hcp** (J/mol)<br>${}^{0}L^{Mg-hcp}_{Mg,Ca}=-401.46-7.53T$ | | | | | This study |
| **Zn-hcp** (J/mol)<br>${}^{0}L^{Zn-hcp}_{Mg,Zn}=-3084.93+5.44T,\ {}^{1}L^{Zn-hcp}_{Mg,Zn}=-6111.27+5.65T$ | | | | | This study |
| **Stoichiometric compounds** | | $\Delta H^{o}_{298.15\ K}$ (J/mol atom) | $S^{o}_{298.15\ K}$ (J/mol atom K) | $C_p$ (J/mol atom K) | |
| IM2 | $(Ca_7Mg_8Zn_{35})$ | −22,320.00 | 33.06 | $7/50C_p$ (Ca, bcc-A2)+$8/50C_p$ (Mg, hcp-A3)+$35/50C_p$ (Zn, hcp-Zn) | This study |
| IM4 | $(Ca_2Mg_{55}Zn_{43})$ | −11,170.00 | 32.24 | $2/100C_p$ (Ca, bcc-A2)+$55/100C_p$ (Mg, hcp-A3)+$43/100C_p$ (Zn, hcp-Zn) | This study |
| | $Mg_{51}Zn_{20}$ | −4746.48 | 35.21 | $51/71C_p$ (Mg, hcp-A3)+$20/71C_p$ (Zn, hcp-Zn) | This study |
| | $Mg_{12}Zn_{13}$ | −10,360.03 | 34.55 | $12/25C_p$ (Mg, hcp-A3)+$13/25C_p$ (Zn, hcp-Zn) | [12] |
| | $Mg_2Zn_3$ | −10,967.24 | 36.33 | $2/5C_p$ (Mg, hcp-A3)+$3/5C_p$ (Zn, hcp-Zn) | [12] |
| | $Mg_2Zn_{11}$ | −9882.95 | 33.08 | $2/13C_p$ (Mg, hcp-A3)+$11/13C_p$ (Zn, hcp-Zn) | [12] |
| | $Ca_3Zn$ | −11,906.31 | 37.78 | $3/4\ C_p$(Ca, bcc-A2)+$1/4C_p$ (Zn, hcp-Zn) | [12] |
| | $Ca_5Zn_3$ | −14,574.42 | 40.53 | $5/8C_p$ (Ca, bcc-A2)+$3/8C_p$ (Zn, hcp-Zn) | This study |
| | CaZn | −17,982.50 | 40.75 | $1/2C_p$ (Ca, bcc-A2)+$1/2C_p$ (Zn, hcp-Zn) | This study |
| | $CaZn_2$ | −22,800.00 | 40.13 | $1/3\ C_p$ (Ca, bcc-A2)+$2/3\ C_p$ (Zn, hcp-Zn) | [12] |
| | $CaZn_3$ | −21,418.76 | 39.0 | $1/4C_p$ (Ca, bcc-A2)+$3/4C_p$ (Zn, hcp-Zn) | [12] |
| | $CaZn_5$ | −19,997.51 | 37.7 | $1/6C_p$ (Ca, bcc-A2)+$5/6C_p$ (Zn, hcp-Zn) | [12] |

system with high accuracy. The isothermal section at 608 K optimized in this work shows significant improvement compared with the model optimized by the previous researchers [11,12]. The improvement is mainly due to the incorporation of the four ternary intermetallic compounds based on the recent experimental data reported by our group [13,35,36].

## 8. Conclusion

Thermodynamic modeling of the Mg–Ca–Zn system has been carried out based on the CALPHAD approach using FactSage software. The thermodynamic modeling of Laves phases in the Mg–Ca and Mg–Zn system, $CaZn_{11}$ and $CaZn_{13}$ in the Ca–Zn system has been carried out. Four ternary intermetallic compounds, IM1, IM2, IM3 and IM4 have been included in the modeling of this system for the first time. Ternary interaction parameters based on the modified quasi-chemical model for the liquid phase have been re-optimized. Experiments were carried out for samples with constant Ca composition (Ca=4 and 6 at%). The results show good agreement between the calculated vertical sections and experimental data from the current work and from the literature over the entire composition range. The current thermodynamic model reproduces the phase relations and solubility ranges in the Mg–Ca–Zn system along the constituent binaries, various vertical sections, liquidus projection and isothermal section at 608 K.

## Acknowledgment

The authors would like to acknowledge Dr. Dmytro Kevorkov and Ahmad Omar Mostafa of the Department of Mechanical and Industrial Engineering, Concordia University for useful discussions and suggestions.

## Appendix A. Supplementary materials

Supplementary data associated with this article can be found in the online version at http://dx.doi.org/10.1016/j.calphad.2014.03.003.

## References

[1] B.L. Mordike, T. Ebert, Magnesium: Properties–applications–potential, Mater. Sci. Eng.: A 302 (2001) 37–45.
[2] I.J. Polmear, Magnesium alloys and applications, Mater. Sci. Technol. 10 (1994) 1–16.
[3] A.A. Luo, Recent magnesium alloy development for elevated temperature applications, Int. Mater. Rev. 49 (2004) 13–30.
[4] B.S. You, W.W. Park, I.S. Chung, The effect of calcium additions on the oxidation behavior in magnesium alloys, Scr. Mater. 42 (2000) 1089–1094.
[5] J.F. Nie, B.C. Muddle, Precipitation hardening of Mg–Ca(-Zn) alloys, Scr. Mater. 37 (1997) 1475–1481.
[6] Y.N. Zhang, X.D. Liu, Z. Altounian, M. Medraj, Coherent nanoscale ternary precipitates in crystallized $Ca_4Mg_{72}Zn_{24}$ metallic glass, Scr. Mater. 68 (2013) 647–650.
[7] Y.N. Zhang, X.D. Liu, Z. Altounian, M. Medraj, Coherent precipitation in melt-spun $Mg_{97.5}Zn_2Ca_{0.5}$ alloy, 2013 (submitted).

[8] B. Zberg, P.J. Uggowitzer, J.F. Löffler, MgZnCa glasses without clinically observable hydrogen evolution for biodegradable implants, Nat. Mater. 8 (2009) 887–891.
[9] E. Ma, J. Xu, The glass window of opportunities, Nat. Mater. 8 (2009) 855–857.
[10] X. Gu, Y. Zheng, S. Zhong, T. Xi, J. Wang, W. Wang, Corrosion of, and cellular responses to Mg–Zn–Ca bulk metallic glasses, Biomaterials 31 (2010) 1093–1103.
[11] C.O. Brubaker, Z.-K. Liu, A computational thermodynamic model of the Ca–Mg–Zn system, J. Alloys Compd. 370 (2004) 114–122.
[12] S. Wasiur-Rahman, M. Medraj, Critical assessment and thermodynamic modeling of the binary Mg–Zn, Ca–Zn and ternary Mg–Ca–Zn systems, Intermetallics 17 (2009) 847–864.
[13] Y.N. Zhang, D. Kevorkov, F. Bridier, M. Medraj, Experimental study of the Ca–Mg–Zn system using diffusion couples and key alloys, Sci. Technol. Adv. Mater. 12 (2011) 025003.
[14] Y.N. Zhang, G.J. Rocher, B. Briccoli, D. Kevorkov, X.B. Liu, Z. Altounian, M. Medraj, Crystallization characteristics of the Mg-rich metallic glasses in the Ca–Mg–Zn system, J. Alloys Compd. 552 (2013) 88–97.
[15] R. Paris, Ternary alloys, Publications scientifiques et techniques du minist'ere de l'air, ministere de l'air, 1934, pp. 1–86.
[16] J.B. Clark, The solid constitution in the Mg-rich region of the Mg–Ca–Zn phase diagram, Trans. Metall. Soc. AIME 221 (1961) 644–645.
[17] J.B. Clark, JCPDS Card 12-569, 1961.
[18] J.B. CLARK, JCPDS CARD 12-266, 1961.
[19] N. Baar, On the alloys of molybdenum with nickel, manganese with thallium, and calcium with magnesium, thallium, lead, copper, and silver, Z. Anorg. Chem. 70 (1911) 362–366.
[20] G. Bruni, C. Sandonnini, The ternary of magnesium, zinc and cadmium II, Z. Anorg. Chem. 78 (1913) 273–297.
[21] G. Bruni, C. Sandonnini, E. Quercigh, The ternary of magnesium, zinc and cadmium, Z. Anorg. Chem. 68 (1911) 73–90.
[22] W. Bulian, E. Fahrenhorst, Solubility of calcium in magnesium, Metallforschung 1 (1946) 70.
[23] R.J. Chadwick, The constitution of the alloys of magnesium and zinc, J. Inst. Metals 449 (1928) 285–299.
[24] G. Grube, Alloys of magnesium with cadmium, zinc, bismuth and antimony, Z. Anorg. Chem. 49 (1906) 72–92.
[25] G. Grube, A. Burkhardt, The electrical conductivity, thermal expansion and hardness of magnesium–zinc, Z. Elektrochem. Angew. Physik. Chem. 35 (1929) 315–331.
[26] J.L. Haughton, Alloys of magnesium. Part 6dthe construction of the magnesium-rich alloys of magnesium and calcium, J. Inst. Metals 61 (1937) 241–246.
[27] W. Hume-Rothery, E.D. Rounsefell, The system magnesium–zinc, J. Inst. Metals 41 (1929) 119–138.
[28] V.P. Itkin, C.B. Alcock, The Ca–Zn system, Bull. Alloy Ph. Diagr. 11 (1990) 328–333.
[29] A.F. Messing, M.D. Adams, R.K. Steunenberg, Contribution to the phase diagram calcium–zinc, Trans. ASM 56 (1963) 345–350.
[30] H. Nowotny, E. Wormnes, A. Mohrnheim, Investigation on the Al–Ca, Mg–Ca, and Mg–Zr systems, Z. Metallkunde 32 (1940) 39–42.
[31] J.J. Park, L.L. Wyman, Phase relationships in magnesium alloys, WADC Technical Report 57-504, 1957, pp. 1–27.
[32] E. Schmid, H. Seliger, Investigation of the solid solutions of magnesium, Metallwirtschaft, Metallwissenschaft, Metalltechnik 11 (1932) 409–412.
[33] W. Schmidt, M. Hansen, Solidus and solvus of the magnesium solid solution of magnesium–zinc alloys, Z. Metallkunde 19 (1927) 452–455.
[34] H. Vosskuhler, The phase diagram of magnesium-rich Mg–Ca alloys, Z. Metallkunde 29 (1937) 236–237.
[35] Y.-N. Zhang, D. Kevorkov, J. Li, E. Essadiqi, M. Medraj, Determination of the solubility range and crystal structure of the Mg-rich ternary compound in the Ca–Mg–Zn system, Intermetallics 18 (2010) 2404–2411.
[36] Y.-N. Zhang, D. Kevorkov, X.D. Liu, F. Bridier, P. Chartrand, M. Medraj, Homogeneity range and crystal structure of the $Ca_2Mg_5Zn_{13}$ compound, J. Alloys Compd 523 (2012) 75–82.
[37] P. Villars, K. Cenzual, Pearson's Crystal Data–Crystal Structure Database for Inorganic Compounds (on CD-ROM), 2010.
[38] O. Reckeweg, C. Lind, A. Simon, F.J. DiSalvo, Reactions of alkaline earth metals and nitrogen in sealed niobium ampoules: the formation of $MgZn_2$ type intermetallic phases in the presence of nitrogen and the new compound $Ba_5[NbN_4]N$, J. Alloys Compd. 384 (2004) 98–105.
[39] D. Sun, H. Enoki, F. Gingl, E. Akiba, New approach for synthesizing Mg-based alloys, J. Alloys Compd. 285 (1999) 279–283.
[40] A. Iandelli, A. Palenzona, Zinc-rich phases of the rare-earth-zinc alloys, J. Less-Common Metals 12 (1967) 333–343.
[41] M. Wendorff, C. Roehr, Polar binary Zn/Cd-rich intermetallics: synthesis, crystal and electronic structure of A(Zn/Cd)13 (A=alkali/alkaline earth) and $Cs_{1.34}Zn_{16}$, J. Alloys Compd. 421 (2006) 24–34.
[42] A.T. Dinsdale, SGTE data for pure elements, Calphad 15 (1991) 317–425.
[43] P.J. Spencer, A.D. Pelton, Y.-B. Kang, P. Chartrand, C.D. Fuerst, Thermodynamic assessment of the Ca–Zn, Sr–Zn, Y–Zn and Ce–Zn systems, CALPHAD: Comput. Coupling Phase Diagr. Thermochem. 32 (2008) 423–431.
[44] F. Sommer, Association model for the description of thermodynamic functions of liquid alloys II, numerical treatment and results, Z. Metallkunde 73 (1982) 77–86.
[45] A.D. Pelton, Y.-B. Kang, Modeling short-range ordering in solutions, Int. J. Mater. Res. 98 (2007) 907–917.
[46] A. Pelton, S. Degterov, G. Eriksson, C. Robelin, Y. Dessureault, The modified quasichemical model I—Binary solutions, Metall. Mater. Trans. B 31 (2000) 651–659.
[47] P. Chartrand, A. Pelton, The modified quasi-chemical model: Part III. Two sublattices, Metall. Mater. Trans. A 32 (2001) 1397–1407.
[48] A. Pelton, P. Chartrand, The modified quasi-chemical model: Part II. Multicomponent solutions, Metall. Mater. Trans. A 32 (2001) 1355–1360.
[49] M. Hillert, The compound energy formalism, J. Alloys Compd. 320 (2001) 161–176.
[50] E.C. Burke, Solid solubility of calcium in magnesium, J. Metals Trans. AIME 203 (1955) 285–286.
[51] F. Kohler, Zur Berechnung der thermodynamischen Daten eines ternären Systems aus den zugehörigen binären Systemen, Monatshefte für Chem. 91 (1960) 738–740.
[52] P. Chartrand, A.D. Pelton, On the choice of "geometric" thermodynamic models, J. Ph. Equilib. 21 (2000) 141–147.